Nan Song
Research Assistant

Dong Qian
Research Assistant

Jian Cao[1]
Assistant Professor

Wing Kam Liu
Professor

Department of Mechanical Engineering,
Northwestern University, Evanston, IL 60208

Shaofan Li
Assistant Professor
Department of Civil and Environmental
Engineering, SEMM Group,
University of California, Berkeley, CA 94720

Effective Models for Prediction of Springback In Flanging

A study on the prediction of springback angle is presented, with focus on the straight flanging operation. The objective of this work is to evaluate the reliability of different methods of prediction. An experiment of straight flanging operation is conducted. Major prediction approaches such as analytical model, numerical simulation using the Finite Element Method (FEM) and the Meshfree Method using the Reproducing Kernel Particle Methods (RKPM) are discussed. A set of sample problems is computed and comparisons are made with the experiment. The numerical analysis shows that the prediction from the 3D meshfree contact code matches well with the data from the FEM 2D solid model. A material property described by the kinematic hardening law provides a better prediction of springback than the isotropic hardening law. [DOI: 10.1115/1.1395019]

Keywords: Metal Forming, Flanging, Springback, Meshfree Method, Kinematic Hardening, Reproducing Kernel Particle Method

1 Introduction

The simulation of manufacturing processes such as sheet metal forming is crucial to reducing design cycle times and time to market. As one of the most common processes for sheet metal, flanging is used to deform the edge of the part to increase the stiffness of the sheet panel and/or to create the mating surface for subsequent assembly. Flanging is performed after the drawing of almost all the sheet metal parts and can have three different in-plane curvatures (straight, concave and convex as shown in Fig. 1 [1]). The shape discrepancy between the fully loaded and unloaded configurations is called springback. The challenge is how to predict the springback angle and thus design a tooling to compensate for the amount of springback.

Efforts to springback prediction of flanging operation have employed both analytical and numerical approaches. For instance, Wang [2] conducted the analytical study by assuming that the bending moment vanishes as the elastic recovery occurs. Monfort and Bragard [3] extended this procedure by using a cantilevered model with a nonuniform moment distribution from the contact point to the outer sheet. Recently, Cao et al. [4] proposed a linear moment distribution in the contact area and that model compares favorably with the experimental results of Liu [5]. The major difficulty with the analytical solution is due to the lack of understanding of the stress distribution throughout the sheet, which limits the analytical approach to simple geometries and simple deformation. Numerical methods are needed for more complicated cases. However, shortcomings in the numerical modeling arise because current finite element-based simulation methods lack the resolution and smoothness to effectively capture the mechanics of the flanging process.

One promising way of circumventing these difficulties is to use meshfree method, a recently developed computational method. The advantage of meshfree method is that it can handle a large variety of material models and account for geometric nonlinearities such as contact. Furthermore, the additional wavelet modes from the meshfree approximation can effectively capture the power of the wrinkling and its post-buckling behavior. Therefore, the effects on the stress state can be accurately accounted for in the simulation.

The objective of this paper is to simulate the flanging operation and springback by using an analytical model, the FEM and the meshfree method using the Reproducing Kernel Particle Methods (RKPM). The contact algorithm in the RKPM method and the computing of springback angle are developed here. Comparison of the data with experimental results for a straight flanging process is given. Investigations are under way for cases where more complex geometries and deformation are involved.

2 Experiment

A schematic of a flanging operation is shown in Fig. 2. A flat blank of thickness t is initially placed between a holder and a die under a binder force of F. The blank will experience elastic-plastic deformation to reach a constrained configuration that consists of a (nearly) straight part l and a curved part S when the punch moves down. Springback occurs as the tooling is removed. Design parameters in the flanging operation include the die radius R, the gap distance g, the flanging length L_0 and the flanging curvature, κ_{out}, in the direction out of the paper plane in Fig. 2, and the material state at flanging, etc. Wrinkling, tearing and surface distortion could happen if the flanging curvature κ_{out} is not infinite (concave flanging or convex flanging).

A straight flanging test was performed on a 150 Ton Computer Controlled HPM Hydraulic Press. The material for the test was AA5182-O, an aluminum alloy commonly used in industry. The material is assumed to follow the power hardening law ($\sigma = K\varepsilon^n$) and the material parameters are listed in Table 1. The blank's size was 150 mm in length, 150 mm in width and 1 mm in thickness with the rolling direction placed in the x direction. Flange lengths of 20 mm and around 10 mm at different gaps ranging from 1.02 mm to 2.1 mm were tested against a die radius of 3 mm. The binder force was set at 460 KN during the flanging process resulting an applied pressure of 20 MPa on the blank and no lubricant was used. Since the die radius and gap sizes are very small compared to the sheet thickness, it is a challenging task to eliminate the noise in the system to obtain the exact relation between springback and gap. Considerable efforts have been made to both control the gap and record the gap correctly. The gap is measured by feeler gauge each time before and after the flanging operation to reach 0.0245 mm in accuracy. Springback angle is

[1]Correspondence author: email: jcao@northwestern.edu

Contributed by the Materials Division for publication in the JOURNAL OF ENGINEERING MATERIALS AND TECHNOLOGY. Manuscript received by the Materials Division July 25, 2000. Guest Editors: Jian Cao and Z. Cedric Xia.

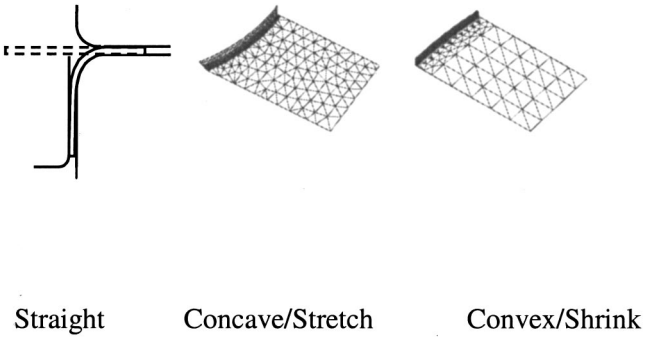

Fig. 1 Schematics of flanging processes

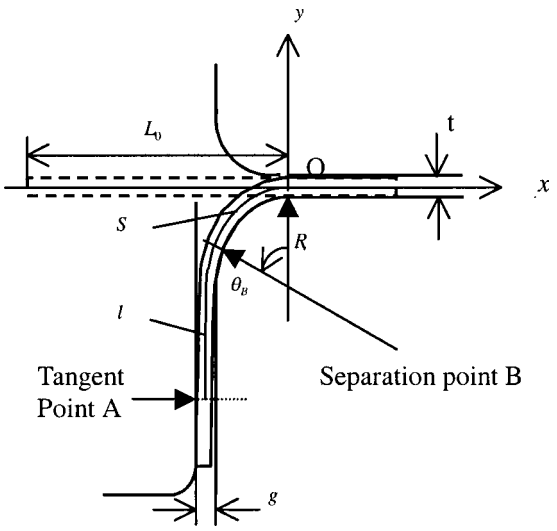

Fig. 2 Schematic of flange operation

Table 1 Material property parameters used in flanging simulation

E	v	σ_y	K	n
70GPa	0.3	146MPa	592MPa	0.306

measured by a Coordinate Measurement Machine (CMM), which results in a 0.09 deg standard deviation. The experiment results are presented in Fig. 6 and Fig. 7.

3 Analytical Model

As reviewed in the introduction section, an analytical model of calculating the springback angle in a straight flanging operation was proposed by Cao et al. [4], which utilized a non-constant moment distribution in the contact zone. The illustration of the analytical model is shown in Fig. 3. The springback angle θ^* can be calculated in a simple way by following Eqs. (1)–(2*a*–*k*). Note that the calculation of springback is only valid when the flange length L_0 is greater than the critical flange length, L_c, defined in Eq. (2*i*–*j*).

$$\theta^* = \theta_l^* + \theta_S^* = a \cdot \left\{ \frac{1}{2} l + \left(1 - \frac{b}{2a} \right) S \right\} \tag{1}$$

where

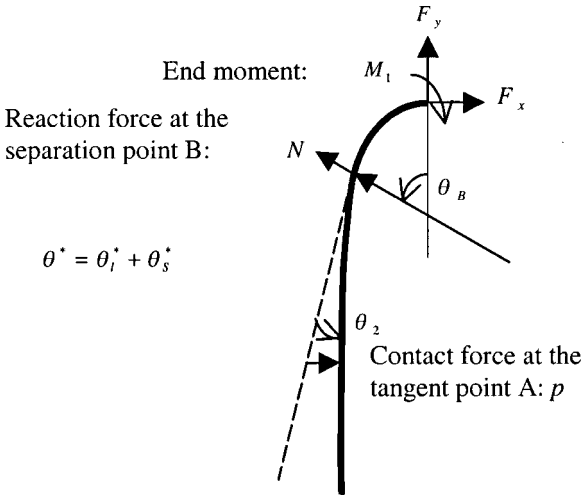

Fig. 3 Illustration of boundary conditions in the analytical model

$$a = \frac{\varphi_0 \gamma_0}{R + \frac{t}{2}}; \tag{2a}$$

$$\frac{b}{a} = \left[\frac{4}{\pi}(1 - M_1') - 2\left(\frac{4}{\pi} - 1 \right) \eta_0 \right] \tag{2b}$$

$$\gamma_0 = \xi_0^{-1} \approx \frac{3}{n+2} \varphi_0^{-n} \tag{2c}$$

$$\varphi_0 = \frac{\sigma_y}{E} \cdot \frac{R + \frac{t}{2}}{\frac{t}{2}} \tag{2d}$$

$$S = \frac{\pi}{2}\left(R + \frac{t}{2} \right) - \eta_0 l \tag{2e}$$

$$l = \frac{\sqrt{g - t} \cdot \sqrt{R + \frac{t}{2}}}{\sqrt{\eta_0 - \psi_0}} \tag{2f}$$

$$\eta_0 \approx \frac{n}{n+1} + \frac{(2+n)(1-n)}{2(1+n)} \varphi_0^{1+n} \tag{2g}$$

$$\psi_0 \approx \frac{n}{2n+1} + \frac{\frac{1}{3} \cdot \frac{1 + 8n^2}{1 + 3n + 2n^2} + \frac{1 - 2n}{1+n} + \frac{1}{3}}{\left(\frac{3}{n+2} \right)^2} \cdot \varphi_0^{1+2n} \tag{2h}$$

$$\delta = \frac{\pi R_p}{2} \quad (R_p = \text{Punch Radius}) \tag{2i}$$

$$L_c = S + l + \delta \quad (L_c: \text{ Critical Flange Length}) \tag{2j}$$

In the above equations, R is the die radius of flanging, R_p is the punch radius, g is the gap between the die and the punch, σ_y is the initial yield stress of the sheet material, E is the Young's modulus, t is the original sheet thickness, and n is the hardening exponent in the power law. The only unsettled parameter in these equations is M_1', i.e.,

$$M_1' = \frac{M_1}{M_B} \quad (0 \leqslant M_1' < 1) \tag{2k}$$

where M_1 is the moment at the origin O and M_B is the moment at the separation point B. This ratio is a function of material properties and flanging geometry, which is under investigation and will be presented in Song and Cao [6].

4 Numerical Simulation Using The Finite Element Method (FEM)

The straight flanging problem (Fig. 2) was modeled using a commercial Finite Element package ABAQUS/standard and simulated as a plane strain problem and therefore, eight-node plane strain solid elements with reduced integration (ABAQUS type CPE8R) and four-node shell elements with reduced integration (ABAQUS type S4R) were employed. A total of 100 elements per layer along the blank were used for both the CPE8R elements with 6 layers through the sheet thickness and the shell elements with 13 integration points through the thickness. The six-layer model was chosen by considering the effect of the number of layers on springback prediction, where the springback angle obtained levels off at a layer number of six. In order to optimize the efficiency of the calculation, the mesh density is 6.6 elements per millimeter in the middle of the blank and reduced to 2 elements per millimeter at the two ends of the blank in the length direction. Due to the fact that this flanging problem is mainly a two-dimensional problem, material parameters used in the yield criterion were determined by matching the tensile test in the rolling direction. Material AA5182-O was modeled by von Mises yield criterion following the power strain hardening law. Both isotropic hardening law and kinematic hardening law are under investigation in this paper. The tooling were treated as rigid surfaces and the friction coefficient was taken to be 0.125 between the tooling and the blank. The boundary and load conditions during flanging process were set to the same condition as in the experiment. The blank was clamped between the holder and the die by 20 MPa in pressure and with free constraints at the ends.

5 Reproducing Kernel Particle Method

5.1 Basic Formulation. Recently, a new generation of numerical methods called ''meshfree'' or ''meshfree method'' has emerged and is now profoundly influencing almost every branch of engineering and the physical sciences. As one part of the meshfree family, the Reproducing Kernel Particle Methods (RKPM) originally evolved from the wavelet theory and SPH method. It has been applied successfully to a broad range of problems. In addition to the SPH and wavelet theory, meshfree method modifies the kernel function by introducing a correction function in order to enhance its accuracy near or on the boundary of the problem domain. Due to this correction function suggested by Liu et al. [7,8], the consistency condition is satisfied. Liu et al. [9] demonstrated the application of meshfree methods to structural dynamics, and the method was used successfully for large deformation simulations [10–13], and computational fluid dynamics [14].

The reproducing kernel particle method can be defined from the following reproducing condition

$$u^R=\int_{x_1}^{x_2} u(y)\kappa_a(x-y)dy=\int_{x_1}^{x_2} u(y)C(x,x-y)\phi_a(x-y)dy \tag{3}$$

The kernel function $\kappa_a(x-y)$ is the product of correction function $C(x,x-y)$ and the window function $\phi_a(x-y)$. The procedure to construct $C(x,x-y)$ is based on the desired accuracy. Here we define the kth moment M_k of the window function as

$$M_K(a,x)=\int_{x_1}^{x_2}(x-y)^k\kappa_a(x,x-y)dy \tag{4}$$

To ensure the reproducing condition be satisfied, one needs

$$M_k(a,x)=\delta_{0,k} \quad \text{for } k=0,1,\ldots,n \tag{5}$$

Construct the correction function using a polynomial basis

$$C(x,x-y)=\sum_{j=0}^{n} b_j(x)(x-y)^j \tag{6}$$

where $b_j(x)$ are the coefficients to be determined.

Enforcing the reproducing condition by Eq. (5) gives

$$\sum_{j=0}^{n} b_j(x)m_{j+k}(a,x)=\delta_{0,k} \quad \text{for } k=0,1,\ldots n \tag{7}$$

Equation (7) gives $n+1$ linear equations for solving the $n+1$ coefficients b_j. In this way, the reproducing kernel can be derived.

In the numerical implementation, the continuous equation (Eq. (3)) needs to be discretized by replacing the integral with a summation.

$$u^R(x)=\sum_{i=1}^{NP} N_I(x)u_I \tag{8}$$

where

$$N_I(x)=\sum_{I=1}^{NP}\left(\sum_{j=0}^{n} b_j(x)(x-x_I)^j\right)\phi_a(x-x_I)\Delta x_I \tag{9}$$

$$u_I=u(x_I) \tag{10}$$

Note that the coefficients b_j are solved in the same way as above by enforcing the moment condition

$$M_k(a,x)=\delta_{0,k} \quad \text{for } k=0,1,\ldots,n, \tag{11}$$

with

$$M_k(a,x)=\sum_{I=1}^{NP}(x-x_I)^k\kappa_a(x-x_I)\Delta x_I=\sum_{j=0}^{n} b_j(x)m_{j+k}(a,x) \tag{12}$$

where Δx_I is the portion of the total length assigned to each node.

The reproducing kernel can be implemented into a Galerkin formulation in a way similar to as in typical finite elements. The major difference in construction is the loop that occurs over nodes instead of elements, but the formulation is almost identical, starting from the weak form of the momentum equation.

5.2 Contact Modeling. The simulation of impact and contact among two or more objects of any kind has always been a challenging problem. It is one of the critical elements in successfully simulating the flanging operation. The major issues that are involved include

1 Geometric Representation: An efficient contact-detection algorithm
2 Kinematic Constraint: Implementation of the so-called impenetration condition with a reasonable constitutive law at contact interface and maintainence of the basic conservation law
3 High-performance Computing: Parallerization.

Numerous contact detection algorithms have been proposed in the literature, such as Benson-Hallquist algorithm, pinball algorithm, Point-in-box, Bounding box, etc. In the context of meshfree method, the moment criterion has been proposed [15]. In this proposed criterion, the determinant of the moment matrix in the context of Reproducing Kernel Particle Method [7] is considered as a natural indicator of the contact condition.

Proposition. For a given domain Ω that has an admissible meshfree distribution, if a spatial point $\mathbf{x}\notin\Omega$ is sufficient away from the domain, the determinant of the moment matrix $\det\{M(x)\}$ evaluated as $\mathbf{x}$ approaches zero, i.e., for given $\delta>0$, $\exists\varepsilon>0$, such that

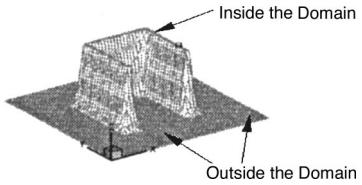

Fig. 4 Profile of det{*M*(*x*)} on a concave region

$$\det\{M(\mathbf{x})\} \leqslant \varepsilon \tag{13}$$

A detailed proof for this proposition has been given in (Li et al. [15]). One might notice that the proposition does not have a strict requirement for the shape of the problem domain, Fig. 4 shows the application of the criterion for a non-convex shape. A plateau is observed for nodes inside the domain and the value of determinant transits to zero as the evaluation point is away from the domain. More testing of the proposed criterion is given in Li et al. [15].

To assure the impenetration condition, we consider the problem of two domains Ω^A and Ω^B with boundary Γ^A and Γ^B, respectively. The momentum equation, the kinematic relation and the constitutive equation are given as

$$\sigma_{ij,j} + b_i = \rho v_i \quad \text{in} \quad \Omega^A \cup \Omega^B \tag{14}$$

$$\dot{\varepsilon}_{ij} = \frac{1}{2}(v_{i,j} + v_{j,i}) \quad \text{in} \quad \Omega^A \cup \Omega^B \tag{15}$$

$$\sigma_{ij}^{\nabla} = \dot{\sigma}_{ij} + W_{ik}\sigma_{kj} + W_{jk}\sigma_{ki} \quad \text{in} \quad \Omega^A \cup \Omega^B \tag{16}$$

where ρ denotes the density; W_{ij} is the anti-symmetric part of the velocity gradient and σ_{ij}^{∇} represents an objective stress increment, e.g., Jaumann stress tensor. The initial conditions of the dependent variables are

$$v_i(0) = v_i^0 \quad \text{in} \quad \Omega^A \cup \Omega^B \tag{17}$$

$$\sigma_{ij}(0) = \sigma_{ij}^0 \quad \text{in} \quad \Omega^A \cup \Omega^B \tag{18}$$

Impenetrability of the two sets Ω^A and Ω^B requires that

$$\Omega^A \cap \Omega^B = 0 \tag{19}$$

A penalty-based method is applied to implement the impenetration condition.

Figure 5 illustrates a typical situation in the 3D contact problem, where $\mathbf{n}_i$ is the outer normal of the *i*th segment of the master element after discretization. $\mathbf{g_n}$ and $\mathbf{g_t}$ denotes the normal and tangential penetrations, respectively. The penalty force along the normal direction of the contact surface is given as

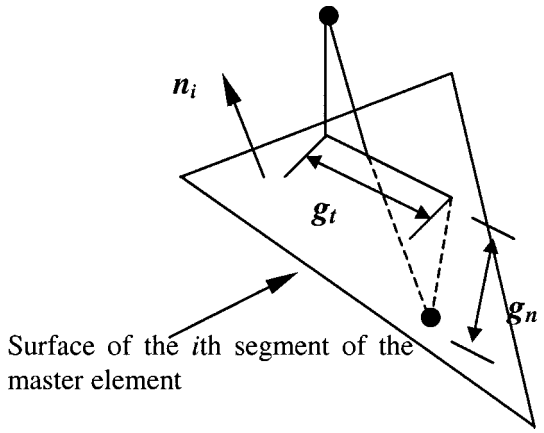

Fig. 5 Contact between a slave node and a surface

$$f_{nj} = \frac{2M_{s(j)}g_{n(j)}}{\Delta t^2}\mathbf{n}_i \tag{20}$$

based on central difference method. In Eq. (20) $M_{s(j)}$ is the lumped mass at j node of the slave body, g_n the normal penetration, Δt the time interval and $\mathbf{n_i}$ the outer normal of the *i*th master segment.

A simple Coulomb friction model is used to consider the effect along the tangential direction, which is given as

$$|f_t| = \min(f_{t1}, f_{t2}) \tag{21}$$

with $f_{t1} = |v_t^i m/\Delta t|$ and $f_{t2} = |\mu_k f_n|$.

The direction of the friction force should be chosen to be opposite the velocity of the corresponding slave node. Our application of this simple approach has shown that it can maintain the impenetration condition fairly well and is stable during the computation.

In summary, the contact algorithm can be outlined as follows:

1 Initialization and discretize the surface into segments
2 Calculate the internal force array
3 Calculate the external force array
4 Use the moment criterion to detect any contact
5 If a contact is detected, compute the normal penetration to further verify the contact
6 Compute the normal and frictional forces and redistribute them to the nodes
7 Get the nodal accelerations
8 Integrate in time to get the velocities and displacements;
9 Return to step 2 until the maximum step number is reached.

5.3 Computation of Springback Angle. An explicit dynamic algorithm has been used in the simulation of the forming process. As the forming is completed, the contact detection on both the upper punch and lower die are terminated. Correspondingly, the constraints from these two parts are released and the sheet starts to springback. To obtain a static solution corresponding to the state of springback, the dynamic relaxation method is adopted. A detailed discussion of the method can be found in Underwood [16]. Chou [17] applied the method in FEM simulation of metal forming. To briefly describe the method, the dynamic equation is considered

$$\mathbf{M}\ddot{\mathbf{u}}^n + \mathbf{C}\dot{\mathbf{u}}^n + \mathbf{f}^{\text{int}}(\mathbf{u}^n) = \mathbf{f}^{\text{ext}}(\mathbf{u}^n) \tag{22}$$

where **M** is the mass matrix, **C** the damping matrix, superscripts ''int'' and ''ext'' denote internal force and external force, respectively, and ''*n*'' is the *n*th time increment. Since a static solution can be seen as a converged result of the dynamic solution, a critical damping coefficient can be used in Eq. (22). In the case of central difference method, the following integrator can be given

$$\dot{u}^{1/2} = \Delta t M \frac{(f^{\text{ext}}(u^0) - f^{\text{int}}(u^0))}{2} \tag{23}$$

for $n = 1$ and

$$\dot{u}^{n+1/2} = \frac{(2 - c\cdot\Delta t)}{(2 + c\cdot\Delta t)}\dot{u}^{n-1/2} + 2hM^{-1}\frac{(f^{\text{ext}}(u^n) - f^{\text{int}}(u^n))}{(2 + c\cdot\Delta t)} \tag{24}$$

for $n > 1$.

To ensure an optimal convergence, numerical experiments are conducted. By checking the responses using different damping coefficients, the critical damping coefficient is chosen for the system. The criterion to stop the dynamic relaxation is given as

$$\|f^{\text{ext}} - f^{\text{int}}\| \leqslant \delta \tag{25}$$

which indicates the equilibrium state is attained.

6 Results and Discussion

Figure 6 illustrates the springback results of various die gaps with a flange length of 20 mm obtained from experiment, the

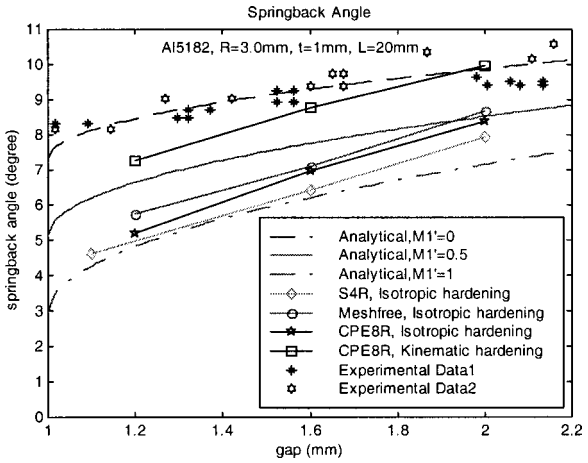

Fig. 6 Springback angle versus gap distance for 20 mm flange length

analytical model, the FEM and the meshfree method. The experimental data shown as stars and hexagrams in Fig. 6 were tested on different dates. It can be seen that springback increases with an increase in gap. The springback angle obtained by the analytical method falls in the area between the line of $M1'=0$ (dashed line in Fig. 6) and the line of $M1'=1$ (dash-dotted line in Fig. 6) depending on the value of M_1' (see Eq. (2)). Notice that experiment data are within the prediction range, however, further investigation on M_1' is needed to provide more precise predictions. It is worthwhile to mention that the mechanics of bending, not just the moment distribution as the focus discussed in this paper, affects the prediction of springback. Many works can be found in literature addressing the bending mechanics issue, for example, the review paper by Huang and Gerdeen [18].

Numerical simulation results are shown as solid lines with different symbols in Fig. 6. It is clear that the S4R elements (diamonds) following the isotropic hardening law give the smallest springback angles and have the largest differences from the experimental results. 2D solid elements (stars) have better predictions, which are expected due to the presence of a small ratio of die radius over sheet thickness ($R/t=3$) in the experiments. The meshfree (circles) method based on the same isotropic hardening law falls in between the predictions obtained from 2D solid elements and shell elements. Further consideration of the Bauschinger effect during unloading is taken into account by employing a kinematic hardening law in the 2D solid element (CPE8R) model. Results obtained by this model (squares) have the best agreement with the experimental data.

General conclusions obtained from observation of Fig. 6 are as follows:

1 Springback angle increases as the gap increases.
2 The FEM with 2D solid elements and meshfree method have better springback predictions than the FEM using shell elements.
3 It is evident that the kinematic hardening law has a better prediction than the isotropic hardening law.
4 Since the current analytical model is based on the isotropic hardening law, further modification of the analytical model by considering the Bauschinger effect may move the $M1'$ limited area upper to a certain level.

Another study on the effect of flange length on springback is show in Fig. 7(*a*) and (*b*). The prediction model is chosen as the 2D solid elements with the kinematic hardening law based on the former conclusions. The springback angles obtained with different flange lengths with two certain die gaps (1.2 mm and 2.0 mm) are shown by solid lines with star symbol in Figs. 7(*a*) and (*b*), respectively. The L_c values marked by ''analytical'' in Fig. 7 are

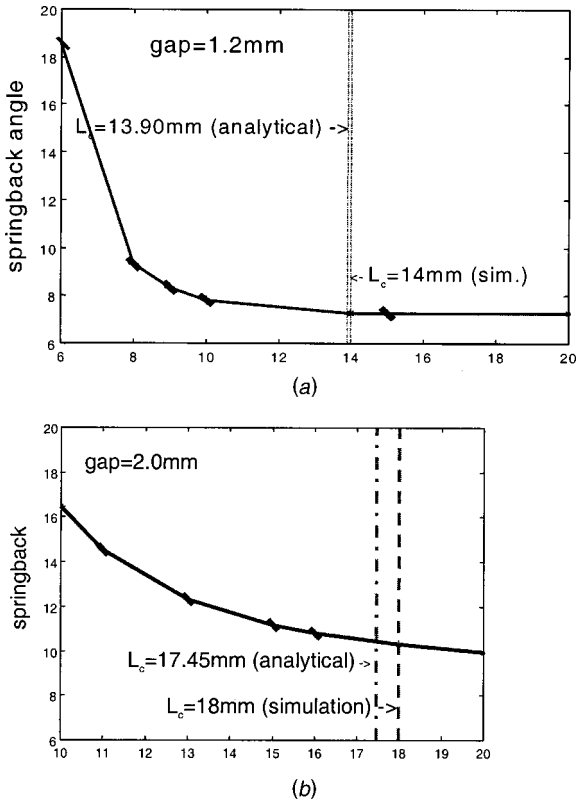

Fig. 7 (*a-b*) Comparison of L_c by numerical and analytical method (*a*) gap=1.2 mm; (*b*) gap=2.0 mm

calculated by Eq. (2*j*). The L_c values marked by ''simulation'' are the approximation data selected by considering the start points when the springback angle levels off in Fig. 7. It shows that the analytical prediction of L_c matches the simulation results well. When the flange length is larger than the critical length L_c, the springback angle is insensitive to the change of the length. On the other hand, when the flange length is smaller than L_c, the springback angle increases rapidly as the flange length decreases. In addition, the critical flange length increases as the gap increases. This indicates that the 20 mm flange length used in Fig. 6, compared to a critical length of 8 mm shown in Fig. 7(*b*), is long enough to neglect the effect of blank length on springback.

Further investigation where the flange length is smaller than L_c is presented in Fig. 8 with different values of gaps and flange lengths. For example, ''L8,g1.2'' shows one case by setting the flange length as 8 mm and the gap between the die and punch as 1.2 mm. Comparison of numerical solutions and experimental data is given. The star symbols in Fig. 8 illustrate the springback angle comparison obtained by experiment and 2D solid elements with the kinematic hardening law while the cross symbols show the angle comparison obtained by experiment and 2D solid element with the isotropic hardening law. The circle symbols show the angle comparison obtained by meshfree method and experiment. If the point falls on the diagonal line in Fig. 8, it means the springback angles obtained by simulation and experiment are the same. If the point falls on the left-upper side of the line, it means that the springback angle obtained from the simulation is larger than the experimental data. According to the springback angles shown in Fig. 8, it can be seen that the simulation solutions have a larger discrepancy with experimental data when the flange length and the gap become smaller (see L7,g1.1 in Fig. 8). Comparing the angles predicted by different methods, the first three conclusions listed above still hold. The predicted springback angle becomes larger if the Bauschinger effect in the material is considered. Finally, the springback angle increases as the flange length

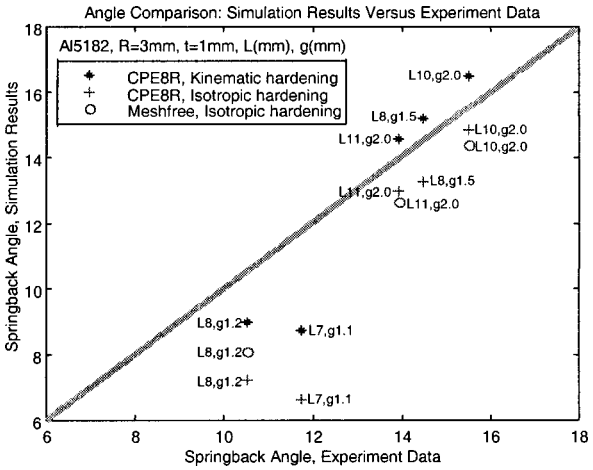

Fig. 8 Angle comparison: simulation results versus experimental data. Different flange lengths and gaps are chosen (L11,g2.0 means: flange length is 11 mm and gap is 2.0 mm).

decreases or as the gap increases as can be seen by comparing (L10,g2.0) with (L11,g2.0) and (L8,g1.2) with (L8,g1.5).

The overall good agreement between numerical simulations with kinematic hardening law provides a solid base for further investigation of springback in convex or concave flanging operation.

Acknowledgment

The financial support for this work from NSF is greatly appreciated.

References

[1] Xia, Z. Cedric, Tang, Sing C., and Carnes, J. C., 1998, ''Accurate springback prediction with mixed solid/shell elements,'' *Simulation of Materials Processing: Theory, Methods and Applications*, Huetink and Baaijens, eds.

[2] Wang, N. M., 1984, ''Predicting the effect of die gap on flange springback,'' *Proceedings of 13th Biennial IDDRG Congress*, Melbourne, Australia, pp. 133–147.

[3] Monfort, G. and Bragard, A., 1985, ''A simple model of shape errors in forming and its application to the reduction of springback,'' *Computer Modeling of Sheet Metal Forming Process: Theory, Verification and Application*, N. M. Wang and S. C. Tang, eds., pp. 273–287.

[4] Cao, J., Liu, Z. H. and Liu, W. K., 1999, ''Prediction of springback in straight flanging operation,'' *Symposium on Advances in Sheet Metal Forming, ASME International Mechanical Engineering Congress and Exposition*, MED-Vol. 10, pp. 921–928.

[5] Liu, Y. C., 1984, ''Springback reduction in U-channels: 'double-bend' technique,'' Journal of Applied Metalworking, **3**, pp. 148–156.

[6] Song, N., and Cao, J., 2001, ''A multi-approach study on springback in straight flanging,'' submitted to ASME J. Appl. Mech.

[7] Liu, W. K., Adee, J., and Jun, S., 1993, ''Reproducing Kernel and Wavelet Particle Methods for Elastic and Plastic Problems,'' *Advanced Computational Methods for Material Modeling*, D. J. Benson and R. A. Asaro, eds., AMD 180/PVP 268 ASME, pp. 175–190.

[8] Liu, W. K., Jun, S., and Zhang, Y. F., 1995, ''Reproducing Kernel Particle Methods,'' Int. J. Numer. Methods Eng., **20**, pp. 1081–1106.

[9] Liu, W. K., Jun, S., Li, S., Adee, J., and Belytschko, T., 1995, ''Reproducing Kernel Particle Methods for Structural Dynamics,'' Int. J. Numer. Methods Eng., **38**, pp. 1655–1679.

[10] Chen, J. S., Pan, C., Wu, C. T., and Liu, W. K., 1996, ''Reproducing Kernel Particle Methods for Large Deformation Analysis of Nonlinear Structures,'' Comput. Methods Appl. Mech. Eng., **139**, pp. 195–228.

[11] Liu, W. K., Chen, Y., Chang, C. T., and Belytschko, T., 1996, ''Advances in Multiple Scale Kernel Methods,'' A special feature article for the 10th anniversary volume of Computational Mechanics, **18**, No. 2, June, pp. 73–111.

[12] Jun, S., Liu, W. K., and Belytschko, T., 1998, ''Explicit Reproducing Kernel Particle Methods for Large Deformation Problems,'' Int. J. Numer. Methods Eng., **41**, pp. 137–166.

[13] Liu, W. K., and Jun, S., 1998, ''Multiple Scale Reproducing Kernel Particle Methods for Large Deformation Problems,'' Int. J. Numer. Methods Eng., **41**, pp. 1339–1362.

[14] Liu, W. K., and Chen, Y., 1995, ''Wavelet and Multiple Scale Reproducing Kernel Methods,'' Int. J. Numer. Methods Eng., **21**, pp. 901–931.

[15] Li, S., Qian, D., Liu, W. K., and Belytschko, T., 2001, ''A Meshfree Contact-detection Algorithm,'' Comput. Methods Appl. Mech. Eng., **190**, pp. 3271–3292.

[16] Underwood, P., 1983, *Computational Methods for Transient Analysis*, Belytschko, T., and Hughes, T. J. R., eds., North-Holland, Amsterdam.

[17] Chou, P. C., and Wu, L., 1986, ''A Dynamic Relaxation Finite-Element Method for Metal Forming Process,'' Int. J. Mech. Sci., **28**, No. 4, pp. 231–250.

[18] Huang, Mai, and Gerdeen, J. C., 1994, ''Springback of Doubly Curved Developable Surfaces—An Overview,'' SAE paper No. 940938, *Analysis of Autobody Stamping Technology*, SP-1021, SAE International Congress, Detroit, MI, pp. 125–138.